PROPAGATION AND MORPHOLOGY OF PRESSURE-CONFINED SUPERSONIC JETS

Michael L. Norman and Karl-Heinz A. Winkler
Max-Planck-Institut für Physik und Astrophysik
Institut für Astrophysik
D-8046 Garching b. München, FRG
and
Larry Smarr
Department of Astronomy
University of Illinois
Urbana, Illinois 61801

1. NUMERICAL JET LABORATORY

The beautiful, high resolution radio maps of jets, lobes, and hot-spots coming off the VLA challenge theorists to explain these phenomena in terms of simple, well-understood physical laws. The difficulty is often not one of finding a reasonable set of physical laws, but of finding their solutions. Analytic solutions of jet structure are limited to steady, isentropic, 1-dimensional flow in channels of slowly-varying cross section; analytic studies of jet stability are limited to modes of small amplitude which, in this regime, assume equal importance as well as unimportance for the gross structure of the flow. Numerical simulation provides a means for investigating those time-dependent, multidimensional, nonlinear solutions that are beyond the reach of analytic tools - solutions that must be relevant to an understanding of astrophysical jets. In an age when computing hardware and software are advancing so rapidly compared to analytic techniques, it is natural to turn to the computer for answers, approximate though they may be.

Numerical solutions can be approximate in several respects, chief of which are:

1) physics: The model system is based on a simplified, incomplete, or inappropriate set of physical laws, either through a desire to study simple cases first, or through ignorance of the correct set of physical laws appropriate to the phenomenon in question. Approximations of this sort are not limited to numerical model-builders.

2) dimensionality: The model system is constructed in a space of reduced dimensionality, either through a desire to study simple cases first, or because the necessary hardware and/or software is not available for the

A. Ferrari and A. G. Pacholczyk (eds.), Astrophysical Jets, 227–251.
Copyright © 1983 by D. Reidel Publishing Company.

higher-dimensional studies. Historically, hardware advances have been accompanied by important innovations in software design (algorithms, etc.). The next generation supercomputer (e.g. CRAY X-MP + SSD) will largely remove the dimensionality limitations of the past in modelling "simple" physics like gas-dynamics, and drive the development of new numerical techniques for more complicated physical systems (e.g. radiation hydrodynamics).

3) accuracy: The model system is further approximated as a discrete system so that it can fit into a finite-sized computer memory. Solutions of the discrete system only approximate to within a certain level of accuracy solutions of the model system. This level of accuracy usually improves as one attempts a finer discretization of the problem (i.e. using more grid points, zones, particles, modes, nodes, elements etc.), but need not improve uniformly over all parts of the solution. Accuracy is a major concern to numerical model builders.

In addition to being approximate, numerical solutions are also incomplete in at least two respects:

1) domain: The numerical solution is found for only a limited region in space-time (you have to cut it off somewhere.)

2) scope: A single numerical solution is a particular solution to the governing equations, and, unlike an analytic solution, does not show dependencies on the fundamental parameters. A family of numerical solutions comprising a parameter search do show dependencies on the basic parameters, however in practice one cannot search parameter space completely.

It is therefore the task of the numerical modeller to extract new qualitative and quantitative information (if any) from approximate and incomplete numerical solutions.

Blandford, Begelman, and Rees, in their 1982 Scientific American article entitled Cosmic Jets, suggest that laboratory investigations of supersonic jets may yield fruitful insights into the cosmic phenomena. They would indeed help, but even laboratory experiments are limited. The advantages of a numerical rather than an experimental approach for problems in fluid dynamics are encapsulated in the 1965 Scientific American article of Harlow and Fromm. They point out that even in cases where laboratory experiments are possible, the numerical approach may be preferred because of cost, flexibility, control of experiment, and accessibility of the data which are free of experimental uncertainties of measurement. Perhaps the most important advantage for understanding astrophysical jets is the ability to control the input physics at will. Here is a case where the appropriate and sufficient set of physical laws is not known, and is in fact one of the objects of inquiry.

Harlow and Fromm's arguments become compelling when one considers the new physical regimes which may exist in jets. Just consider the cost

involved in studying relativistic jets in the laboratory! Indeed, the comprehensive experimental study of axisymmetric, supersonic jets by Love et al. (1959) encompasses only flow Mach numbers between 1 and 3, and describes only jets that are far out of pressure equilibrium with their surroundings. One advantage that laboratory experiments currently do have is that they are 3-dimensional, but rapid advances in computing hardware and software are eroding that advantage as well. Thus, we have undertaken a program to study basic jet physics in a numerical laboratory.

2. THEORETICAL PLANE

The problem we consider is the time-dependent penetration of a collimated, supersonic beam of gas into a constant ambient gas. The numerical experiments described here extend earlier work of this nature we reported in Norman, Smarr, Winkler, and Smith (1982; hereafter NSWS). The reader is referred to NSWS for a more complete description of our physical and numerical assumptions, as well as a comparison of our computer code against a flow measured in the laboratory. Here we shall only review our program and assumptions against the framework established in section 1.

physics: We assume ideal, nonrelativistic gas dynamics; adiabatic flow; $\gamma = 5/3$ ideal gas EOS for both jet and ambient medium. Beam is introduced with zero opening angle and with equal pressure to the undisturbed medium. Jets thus produced are members of a 2-parameter family, which we take to be 1) ratio of beam density to medium density ρ_b/ρ_m, and 2) beam Mach number M_b. By choosing a constant, static ambient medium, we have eliminated "environmental effects".

dimensionality: Flow is assumed to be symmetric about the jet axis, thus we deal in 2 space + 1 time dimensions. Potentially important non-axisymmetric structures and modes of instability are therefore not modelled.

accuracy: The numerical method we use is described in Norman and Winkler (1983), and is shown to compare favourably in accuracy with the BBC scheme on a series of standard test problems devised by Woodward and Colella (1983). Our method and the BBC scheme are generically similar; both are explicit, artificial viscosity methods for computing 2-dimensional flows with strong shocks. We compute with an Eulerian mesh of $75 \times 640 = 48{,}000$ zones, which allows adequate resolution of shocks and surface instabilities that develop in the flow. Sensitivity of our results to 1) zoning resolution, 2) order of accuracy, and 3) use of a material interface on the jet boundary are also discussed in Norman and Winkler (1983).

domain: Spatial domain comprises $0 \leq Z \leq 80$ (640 uniform zones), $0 \leq R \leq 15$ (60 uniform zones out to $R = 7.5$, 15 ratioed zones beyond). We evolve forward in time until the jet has propagated to $Z = 80$. The

beam is admitted with a radius R_b = 1., thus jets up to 40 times their diameter can be studied.

scope: Our numerical survey consists of 12 evolutions parameterized by the various combinations of ρ_b/ρ_m = 0.01, 0.1, 1.0, 10. and M_b = 1.5, 3., 6., 12. shown in Figure 1.

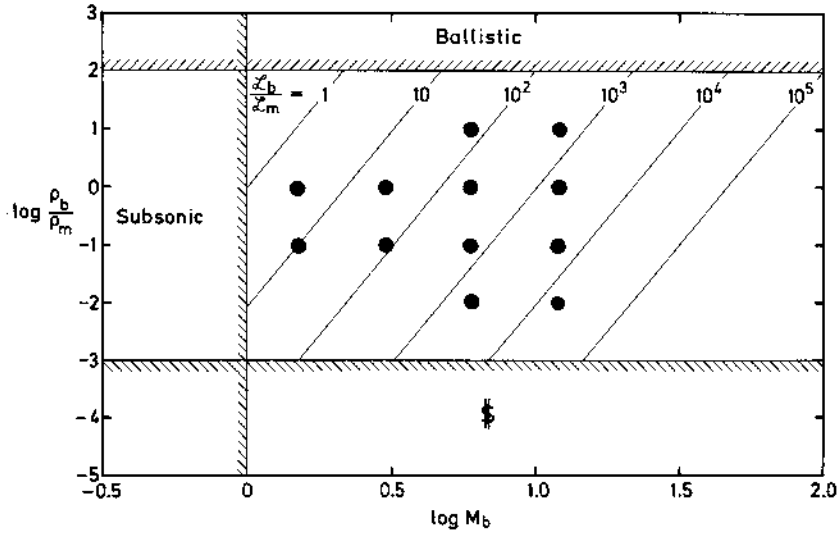


Figure 1. Density ratio - Mach number plane, and the location of the 12 evolutions presented here (large dots). Lines of constant beam kinetic luminosity $\mathcal{L}_b = \frac{\pi}{2} R_b^2 \rho_b V_b^3$ in units of the ambient medium $\mathcal{L}_m = \frac{\pi}{2} R_b^2 \rho_m C_m^3$ are shown in light. Hatched lines bound regions not considered for reasons given in the text.

Lines with hatchmarks indicate regions of the theoretical plane which have not been considered. Although an investigation of subsonic jets is probably necessary to understand wide-angle-tails and low luminosity jet morphologies, we do not consider $M_b < 1$ because 3D effects dominate in this regime (e.g. turbulence). We arbitrarily define $\rho_b/\rho_m > 10^2$ to be the ballistic regime, and do not consider it because there are better ways to do ballistics than with a hydro code (e.g. Hjellming and Johnston 1981). The region $\rho_b/\rho_m < 10^{-3}$ has not been investigated because of the prohibitive computational costs involved, despite the fact that astrophysical jets may be highly diffuse.

3. ARCHIVE OF PROPAGATING JETS

We have surveyed the "allowed" region of the theoretical plane (Figure 1) to the extent where we believe the essential dependencies of jet behavior on the beam parameters emerge. The 12 evolutions comprising this survey are archived here and analyzed in the following sections. We include this archive because 1) there is a general need for more complete documentation of numerical experiments than is now customary, and 2) each of the 12 evolutions is rather different from the others. By thus providing the data base from which our understanding of the flows is drawn, the interested reader is invited to make his own interpretations which can be compared with our own.

There remains, however, the problem of extracting useful information from the mountains of numbers the computer has produced, and presenting this information in a form that is transparent and unambiguous to the numerical modeller and interested reader alike. The problems of extracting and displaying information are often one and the same as the amount of data becomes large. One then speaks of image processing instead of plotting.

The traditional mode of display for a 2-dimensional flow field is to plot isocontour lines of density, temperature etc. with or without flow vectors superposed. We find this medium to be of limited use for clarifying very complicated flow fields involving many extrema, or simply to be an inappropriate medium for asking certain questions of the flow. The questions we ask here are 1) what is the kinematic structure of the jet?, 2) how does this depend on location in the theoretical plane?, and 3) how does the jet propagate?, i.e. rate of advance, flow stability etc. Questions of internal shockwave structure, working surface dynamics, and entrainment will be considered in separate future papers.

A mode of display which we find useful for elucidating kinematic structure and which is used in this archive is illustrated in Figure 2. As axisymmetry is assumed, the image has been mirrored through the jet axis.

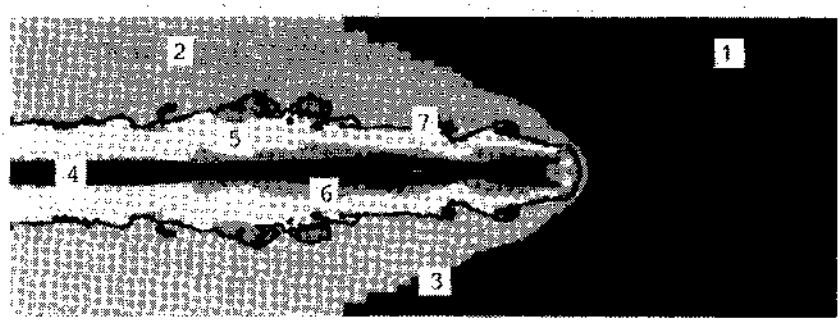


Figure 2. Kinematic structure of a supersonic jet (ρ_b/ρ_m = 0.01, M_b= 12). Seven distinct flow entities are labeled and defined in the text.

Different shades of grey represent parts of the flow having distinct identities or being in particular states of motion. These are labeled in figure 2 and have the following meanings: 1) undisturbed confining medium, 2) disturbed confining medium, 3) bow shockwave, 4) beam (defined where $\rho v_{\parallel}^3 > 5\%$ of the largest $\rho v_{\parallel}^3$ in the jet), 5) backward-flowing cocoon gas ($v_{\parallel} < 0$), 6) forward-flowing cocoon gas ($v_{\parallel} > 0$), and 7) contact discontinuity.

The images themselves are produced with a RAMTEK Color Display System, and recorded with a MATRIX INSTRUMENTS Color Graphic Camera. The display monitor has a raster field of 512 × 512 pixels, each 16 bits deep. Operationally, the flowfield is analysed zone by computational zone, each of which is assigned an integer between 1 and 7 according to the above criteria. The zone is then mapped into the raster field where its associated pixel(s) are illuminated with the color or grey tone assigned to its integer. Since the number of computational zones along the jet axis (640), exceeds the number of pixels (512), the images slightly under-resolve the data behind them.

The 12 evolutions presented in Figures 3-14 are grouped according to Mach number, in order of increasing beam kinetic luminosity. The dimensionless luminosity parameter $(\rho_b/\rho_m)^{-1/2} M_b^3$ varies by almost 4 orders of magnitude in this survey (cf. Figure 1). Each figure shows the jet at 4 stages of development chosen at regular length intervals. Each image covers the entire computational domain ($0 \leq Z \leq 80$, $0 \leq R \leq 15$) plus its mirror image. The beam is continuously admitted at left with radius $R_b = 1$ with the parameters indicated, and with the pressure of the undisturbed ambient gas. Boundary conditions are described in NSWS.

4. PROPAGATION EFFICIENCY

Define propagation efficiency η as the ratio of the actual velocity U of the head of the jet and usual ram-pressure estimate $U_{rp}=V_b(1+\rho_m/\rho_b)^{-1}$, where V_b is the beam velocity and ρ_b/ρ_m is the density ratio. η will in general be less than unity because U_{rp} is derived assuming a steady, head-on momentum transfer between the beam and the ambient medium over the entire area of the working surface, whereas the flow there is manifestly multidimensional(Blandford and Rees, 1974; NSWS), as well as time-dependent (NSWS).

In Table 1 we list 2 sets of propagation velocities and efficiencies for the 12 jets in our survey. The first set U_{av} and η_{av} are average values, where U_{av} is computed by dividing the total distance the jet has travelled by its evolutionary age in Figures 3d-14d. The second set U_e and η_e are end values, where U_e is similarly computed between Figures 3c-14c and 3d-14d. We further define a deceleration parameter $\delta \equiv \rho_e - \rho_{av}$.

An examination of these simply-defined quantities in Table 1 yields the following basic dependencies on the beam parameters:

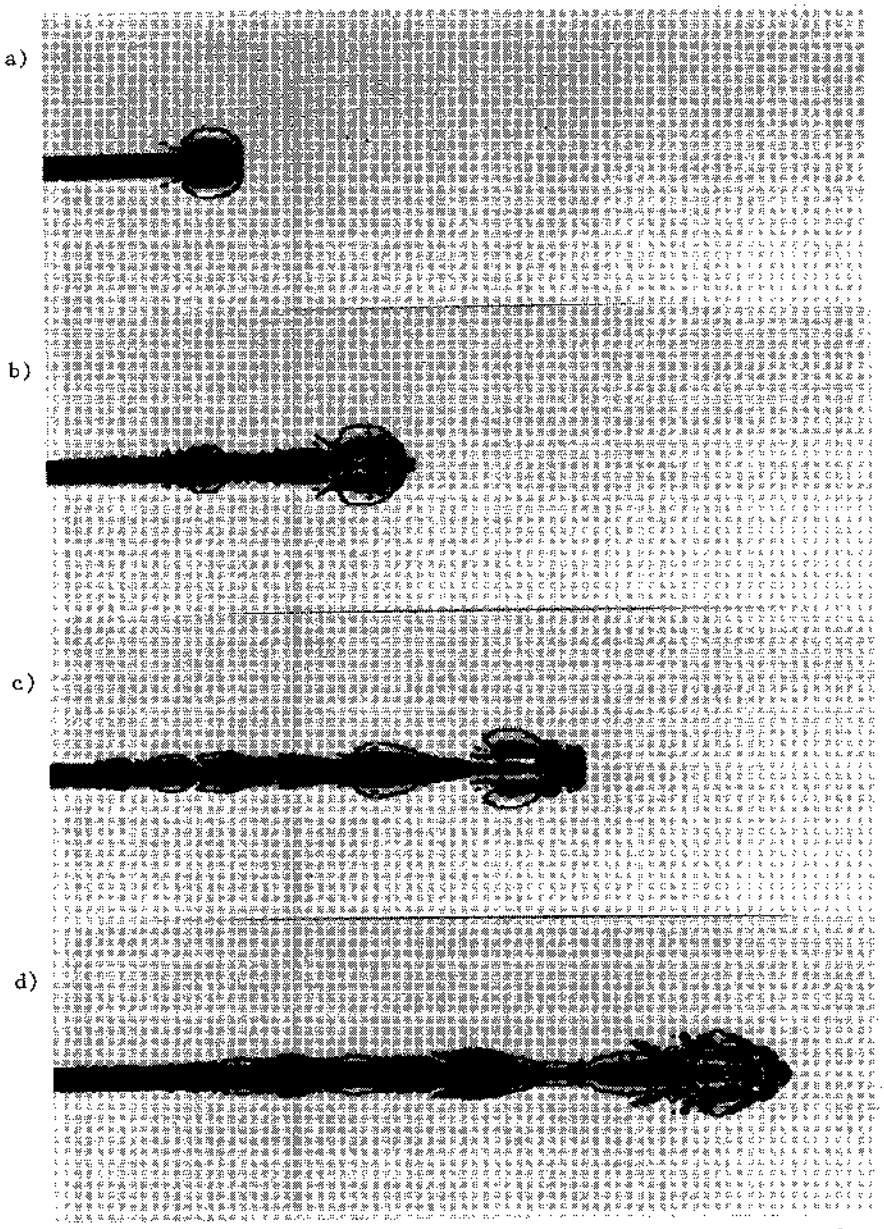


Figure 3. (ρ_b/ρ_m = 1, M_b = 1.5) Kinematic structure at 4 evolutionary times a) t = 30, b) t = 54, c) t = 78, d) t = 108. Jet advances subsonically, therefore no bowshock is present.

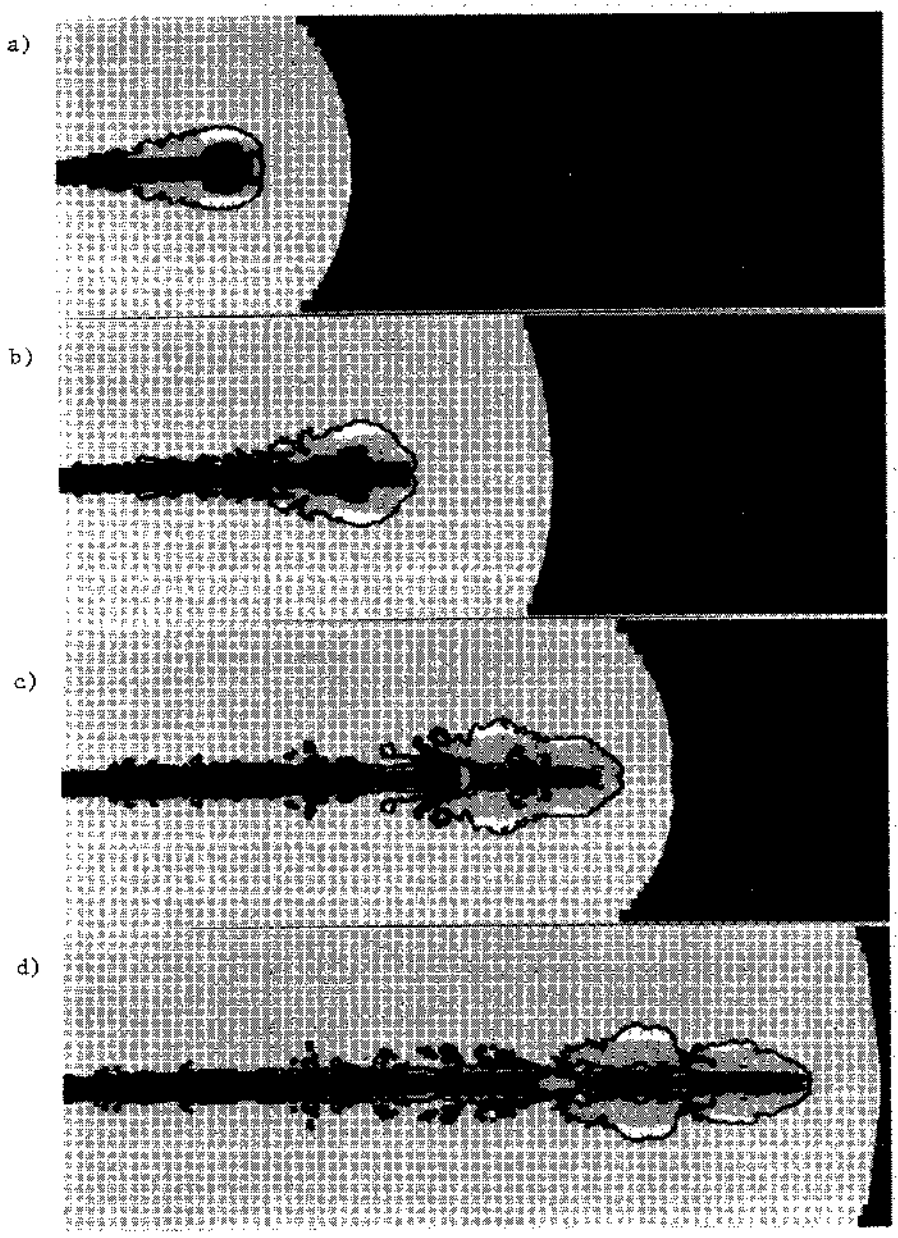


Figure 4. (ρ_b = 0.1, M_b = 1.5) Kinematic structure at 4 evolutionary times: a) t = 24, b) t = 42, c) t = 63, d) t = 81.

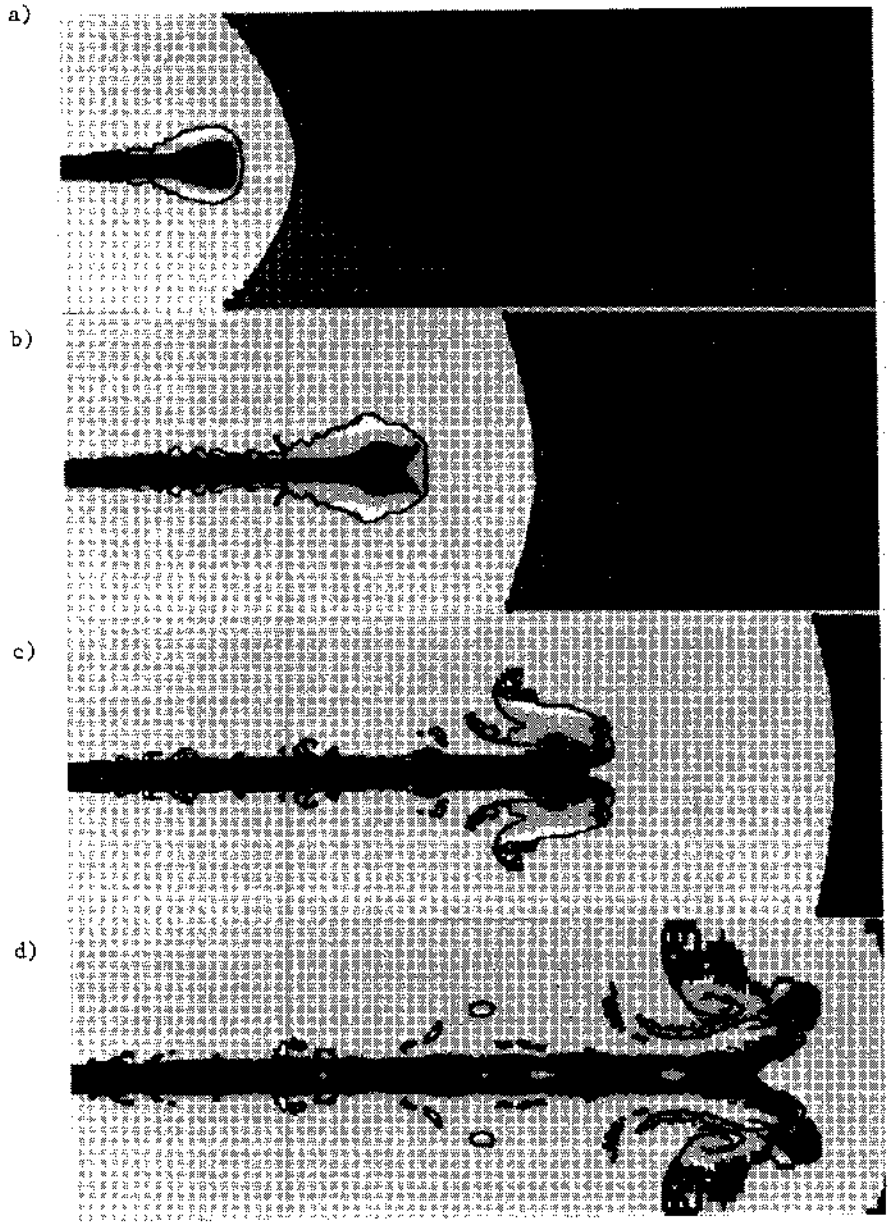


Figure 5. (ρ_b = 1, M_b = 3) Kinematic structure at 4 evolutionary times. a) t = 16, b) t = 36.5, c) t = 64, d) t = 100.

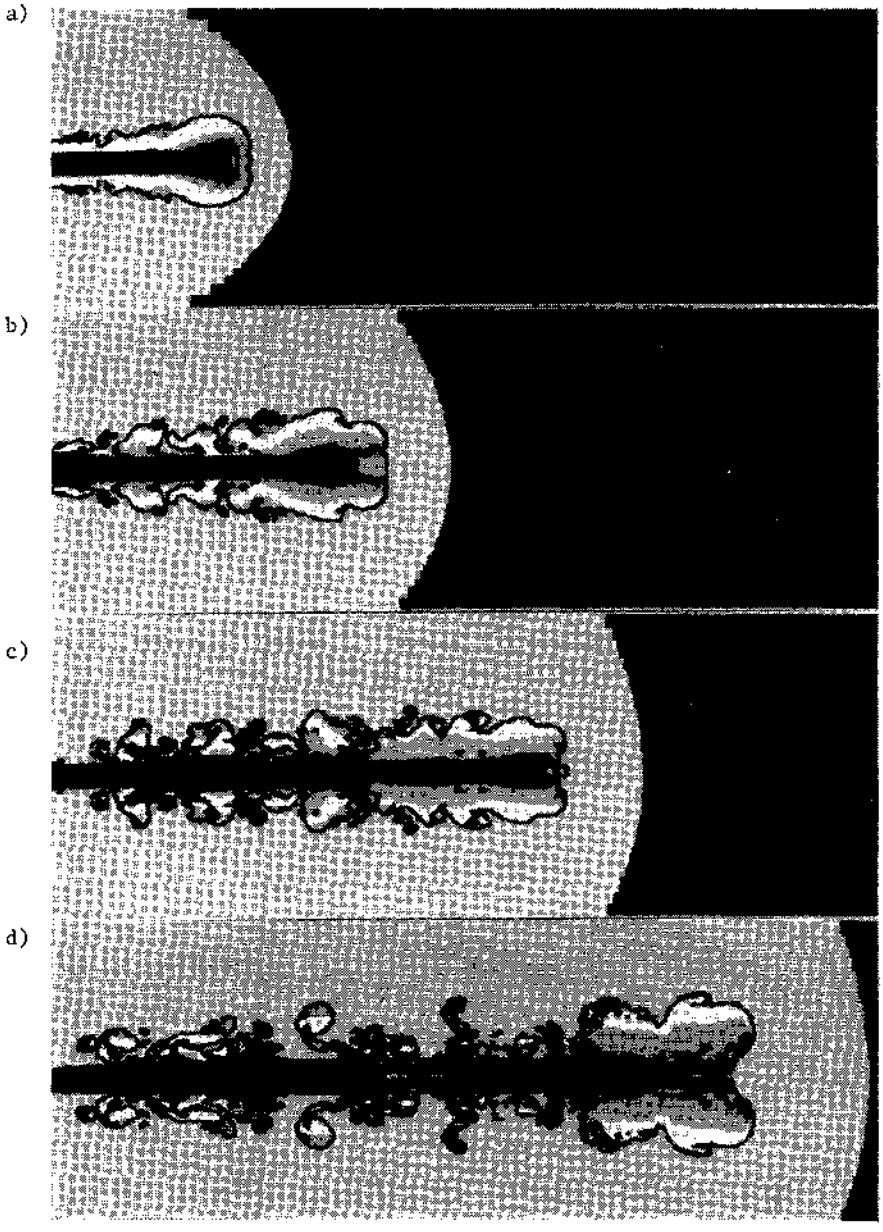


Figure 6. (ρ_b = 0.1, M_b = 3) Kinematic structure at 4 evolutionary times. a) t = 13, b) t = 25, c) t = 41, d) t = 60.

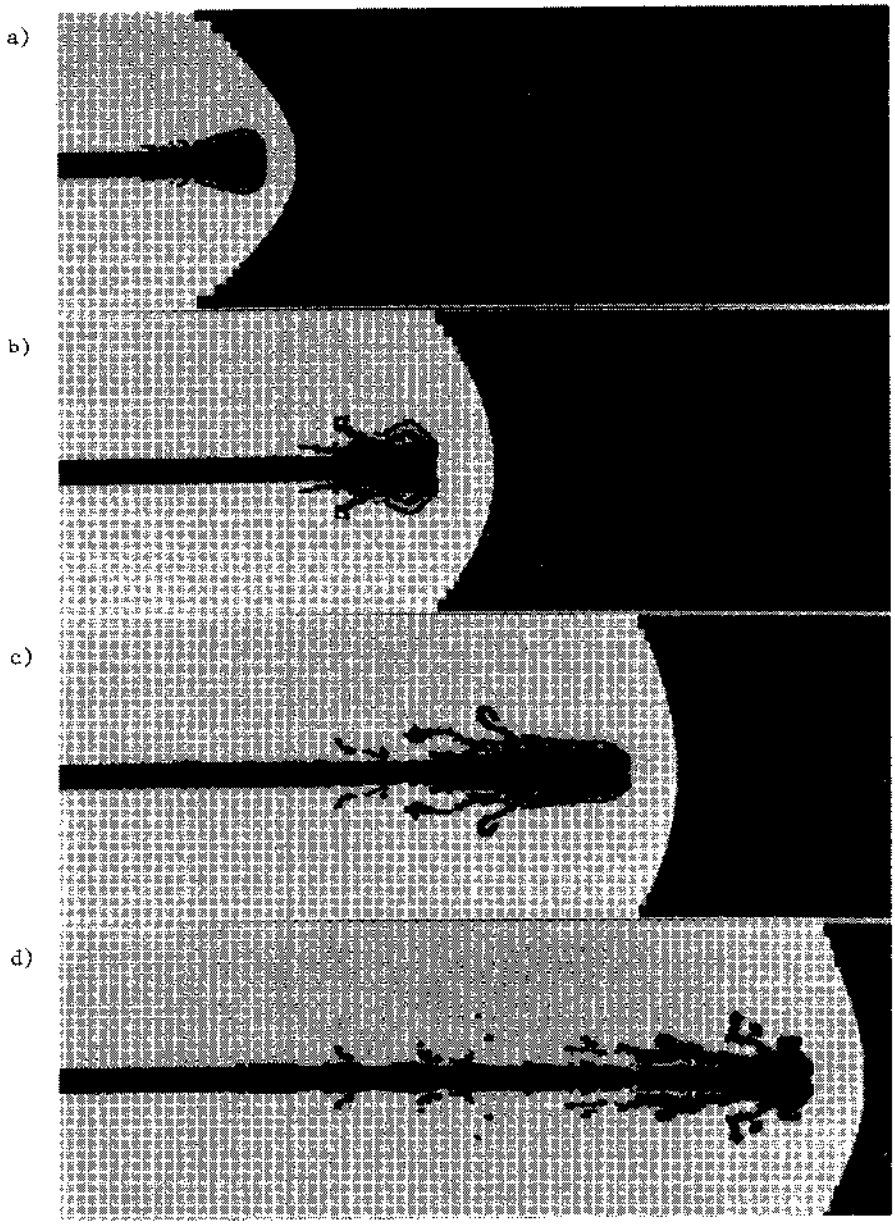


Figure 7. (ρ_b = 10, M_b = 6) Kinematic structure at 4 evolutionary times: a) t = 15, b) t = 30, c) t = 45, d) t = 60.

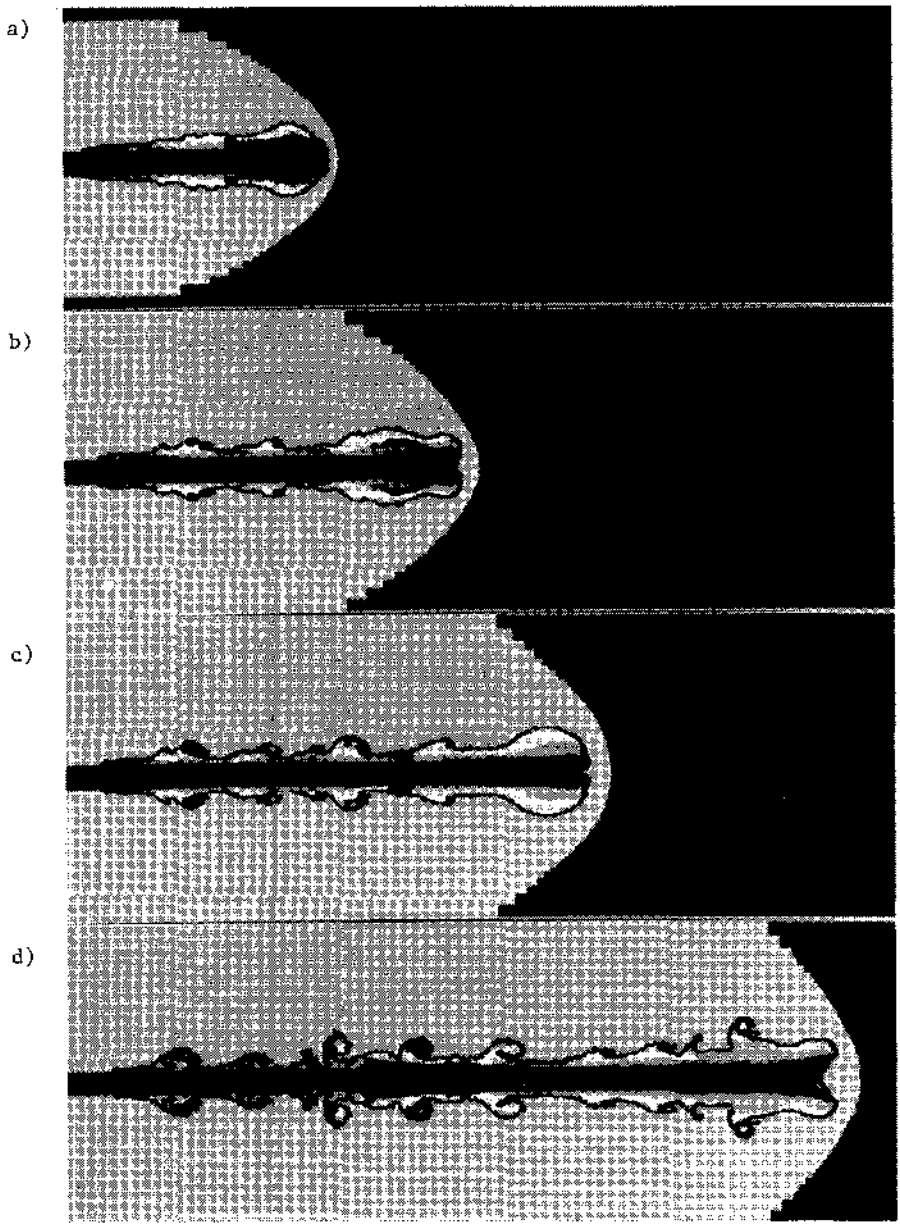


Figure 8. (ρ_b = 1, M_b = 6) Kinematic structure at 4 evolutionary times. a) t = 10, b) t = 16, c) t = 22, d) t = 34.

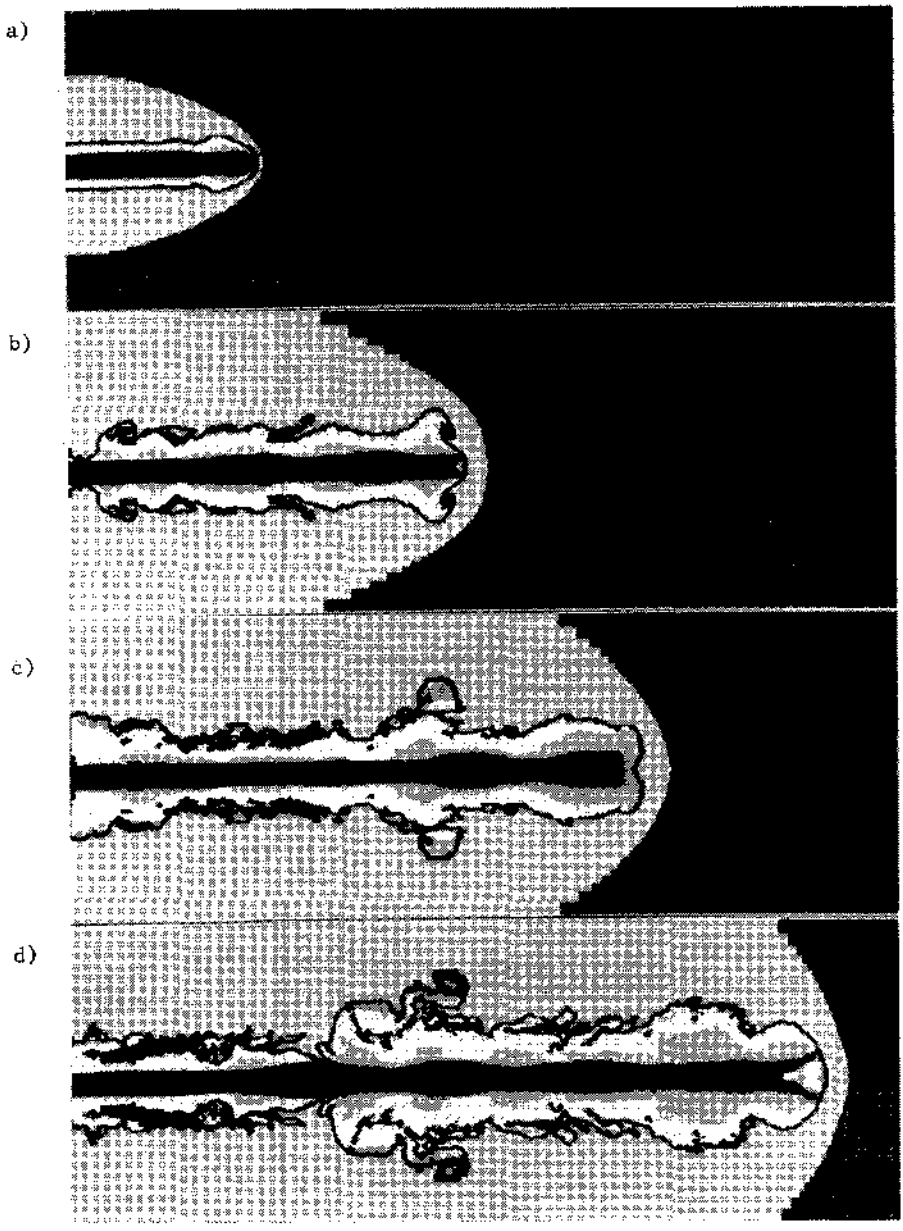


Figure 9. (ρ_b = 0.1, M_b = 6) Kinematic structure at 4 evolutionary times. a) t = 4, b) t = 11, c) t = 18, d) t = 27.

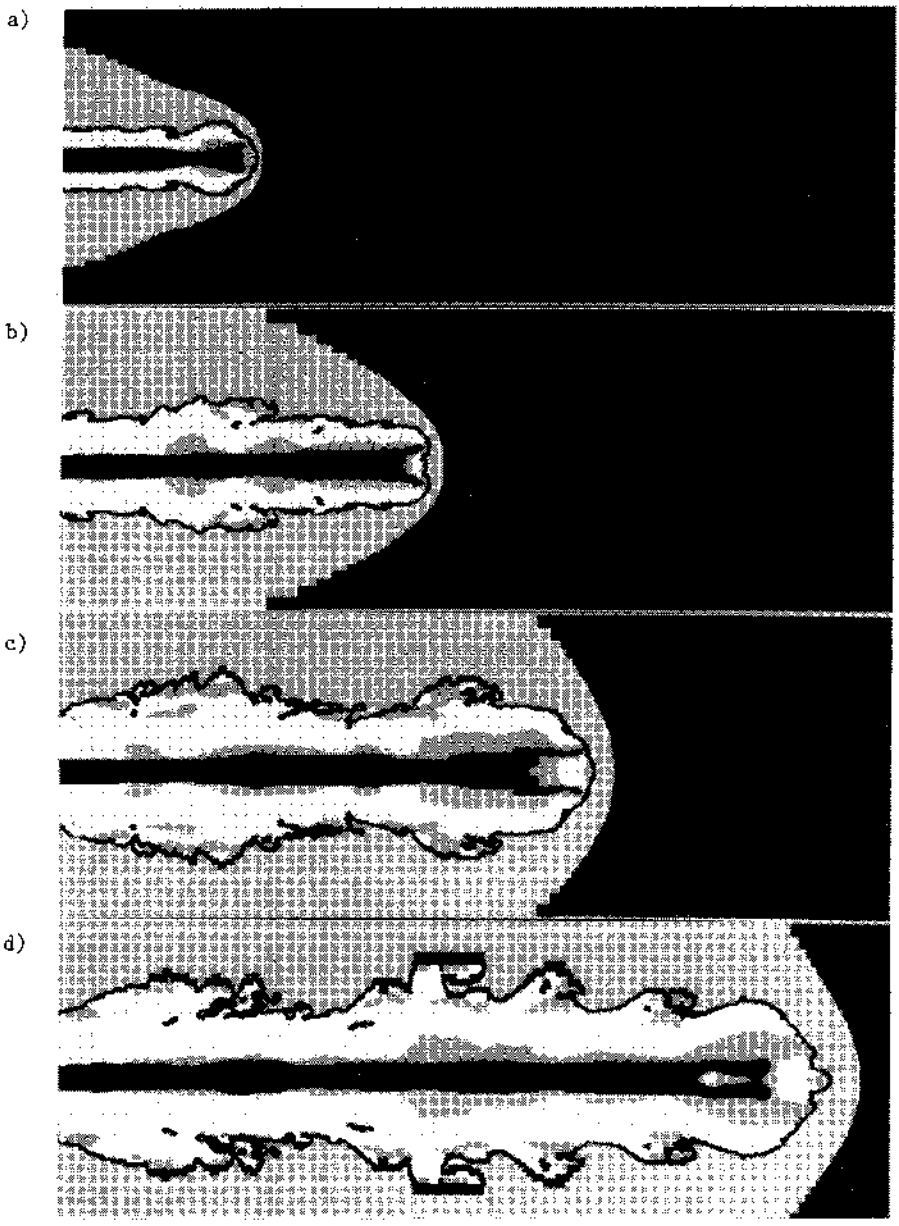


Figure 10. (ρ_b = 0.01, M_b = 6) Kinematic structure at 4 evolutionary times. a) t = 3, b) t = 8, c) t = 15.3, d) t = 27.

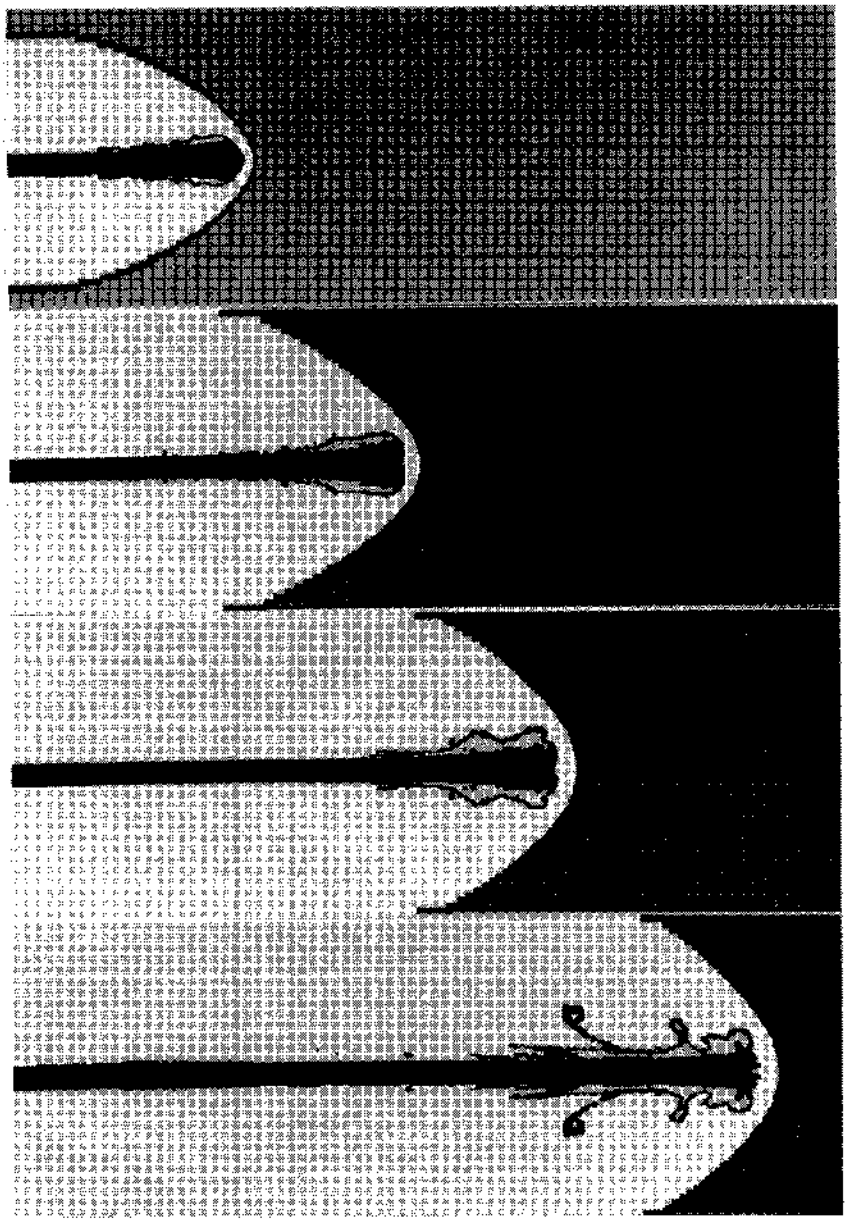


Figure 11. (ρ_b = 10, M_b = 12) Kinematic structure at 4 evolutionary times. a) t = 8, b) t = 14, c) t = 20, d) t = 28.

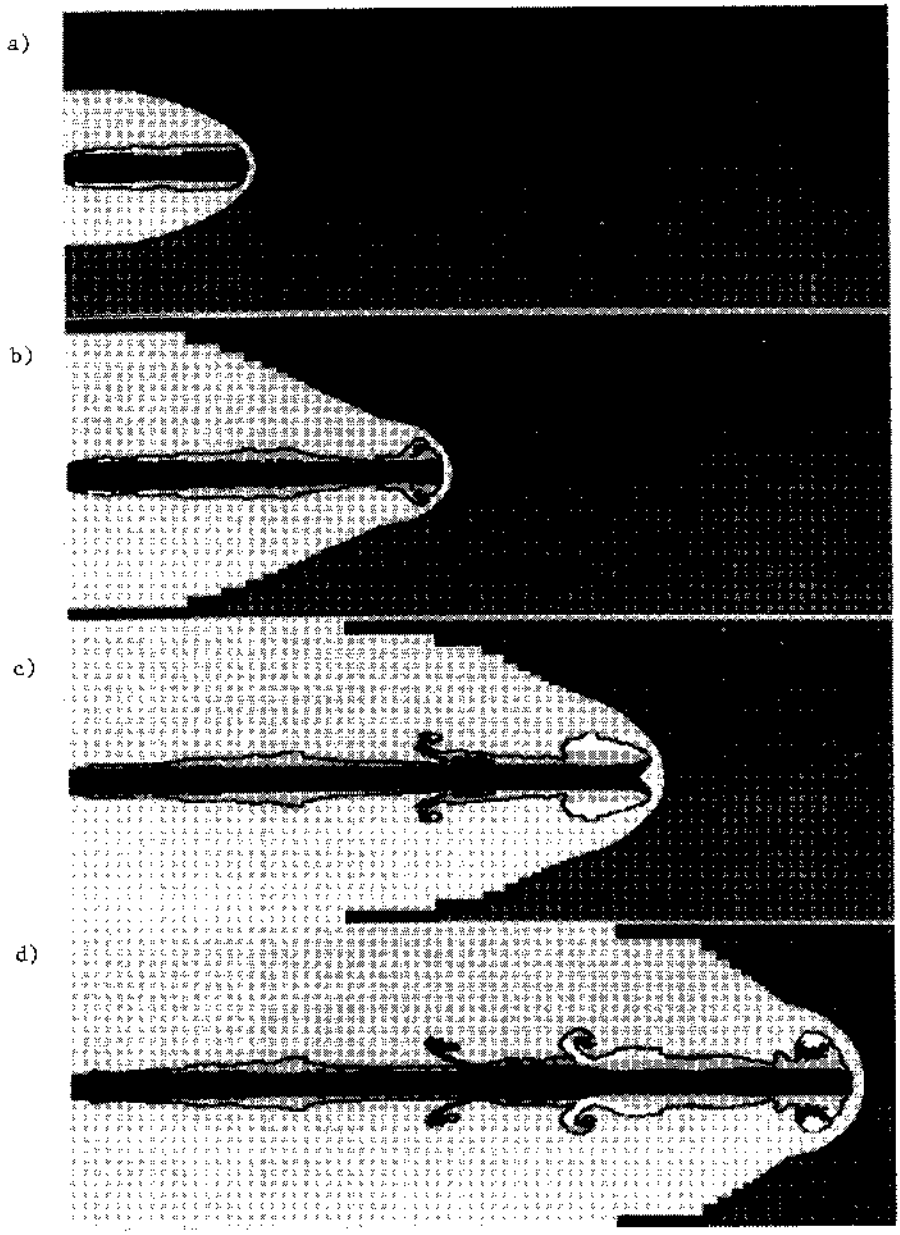


Figure 12. (ρ_b = 1, M_b = 12) Kinematic structure at 4 evolutionary times. a) t = 3, b) t = 6, c) t = 10, d) t = 14.

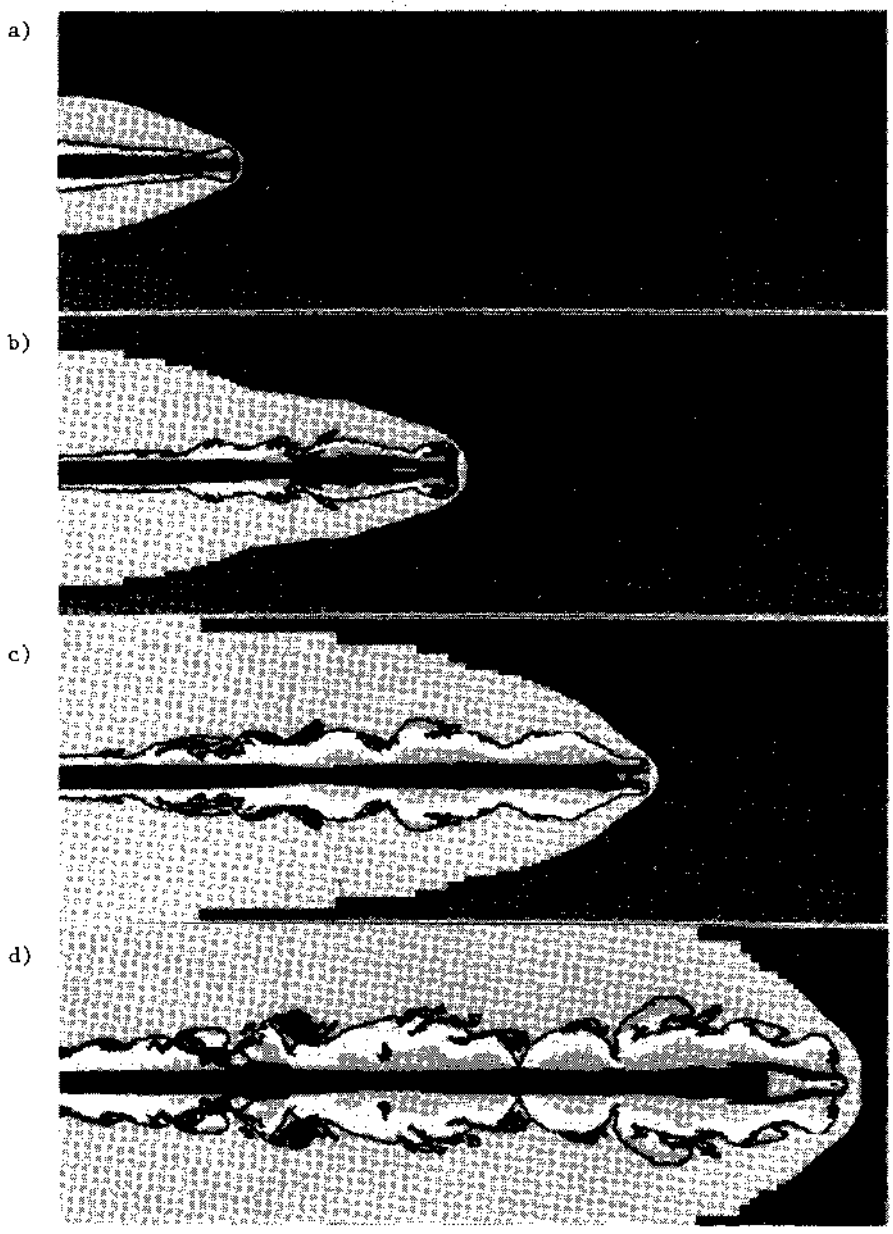


Figure 13. (ρ_b = 0.1, M_b = 12) Kinematic structure at 4 evolutionary times. a) t = 1.5, b) t = 3.5, c) t = 6, d) t = 10.

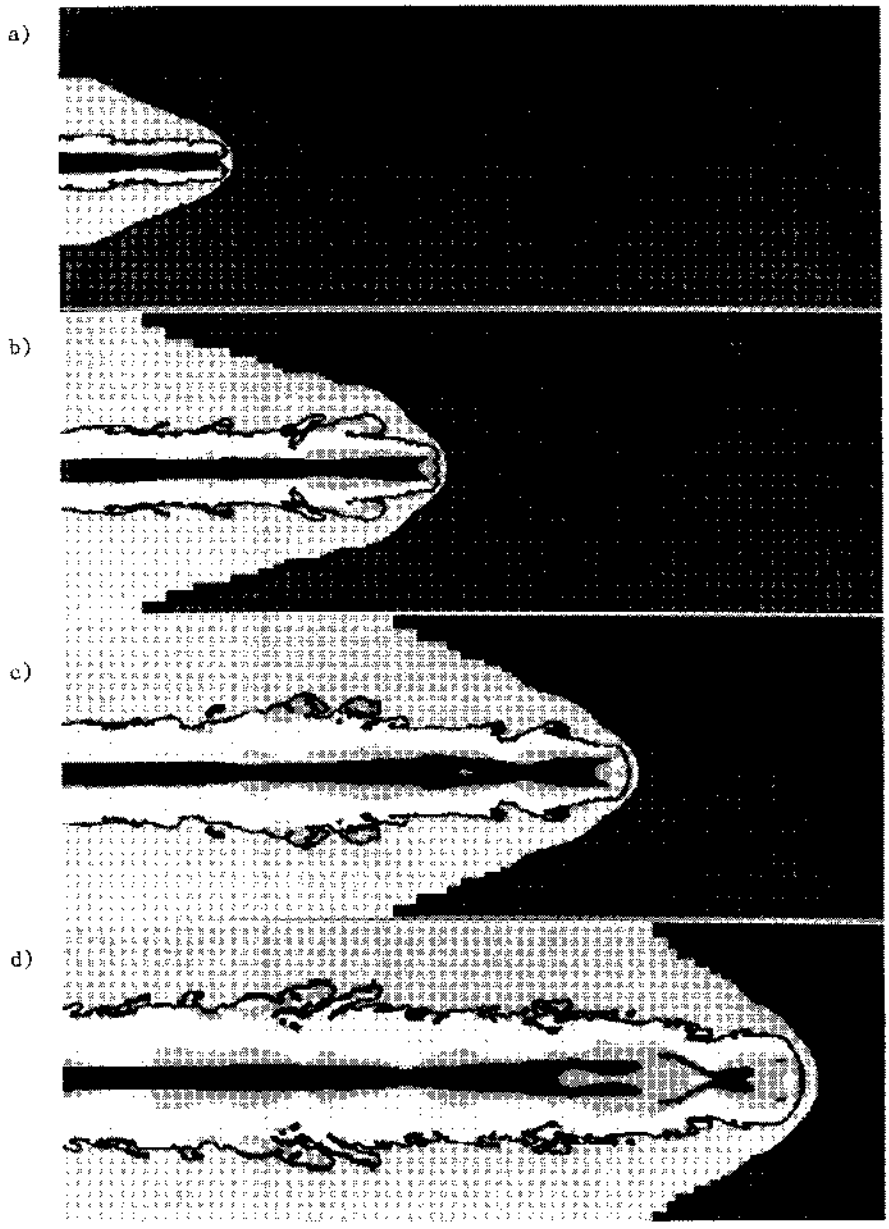


Figure 14. (ρ_b = 0.01, M_b = 12) Kinematic structure at 4 evolutionary times. a) t = 1, b) t = 3, c) t =5 , d) t = 7.6.

Table 1. Propagation velocities and efficiencies*

ρ_b/ρ_m	M_b	V_b	U_{rp}	U_{av}	η_{av}	U_e	η_e	δ
0.01	6	60	5.4	2.77	.51	1.97	.36	−.15
	12	120	10.8	9.47	.88	6.42	.59	−.29
0.1	1.5	4.75	1.14	0.89	.78	0.98	.86	+.08
	3	9.5	2.28	1.13	.50	0.94	.41	−.09
	6	19	4.56	2.70	.59	1.96	.43	−.16
	12	38	9.12	7.65	.84	4.88	.54	−.30
1.0	1.5	1.5	0.75	0.66	.88	0.66	.88	0
	3	3	1.5	0.73	.49	0.56	.37	−.12
	6	6	3	2.18	.73	1.96	.65	−.08
	12	12	6	5.42	.90	4.80	.80	−.10
10.	6	1.9	1.44	1.21	.84	1.17	.81	−.03
	12	3.8	2.88	2.57	.89	2.39	.83	−.06

* Column headings: 1) density ratio, 2) Mach number, 3) beam velocity, 4) ram-pressure estimate for velocity of jet advance, 5) average velocity of jet advance, 6) average propagation efficiency $\equiv U_{av}/U_{rp}$, 7) end velocity of jet advance, 8) end propagation efficiency $\equiv U_e/U_{rp}$, 9) deceleration parameter $\equiv \eta_e - \eta_{av}$.

1) Holding ρ_b/ρ_m fixed, η is high for $M_b = 1.5$, reaches a minimum around $M_b = 3$, and then increases as M_b increases.
2) Holding M_b fixed, η increases as ρ_b increases.
3) δ increases as M_b increases.

Note trends 1) and 2) hold true for both η_{av} and η_e. The most efficient propagators are the dense ($\rho_b/\rho_m \geq 1$), high Mach number ($M_b \geq 6$) jets, and curiously the $M_b = 1.5$ jets; both have $\eta \approx 0.8$. The least efficient propagators are diffuse ($\rho_b/\rho_m < 1$) jets of low to moderate Mach numbers ($3 \lesssim M_b \lesssim 6$), with $\eta \lesssim 0.4$.

Propagation efficiency is closely correlated to the gross morphology of the jet, which is the next topic we wish to consider.

5. FLOW KINEMATICS AND GROSS MORPHOLOGY

Having described how jets of different properties move, we now consider how they appear. We attempt to relate a jet's gross morphology to its underlying flow structure, and examine how these depend on beam density and Mach number as well as evolutionary age.

The most striking morphological dependence is that of jet width on beam density for high Mach number jets ($M_b \geq 6$). This dependence is illustrated in Figure 15 for a sequence of Mach 6 jets. At high densities (Fig.15a), the beam is in direct contact with the external medium and feeds a working surface that leaves behind dense filaments. At equal densities (Fig.15b) the beam is surrounded by a thin cocoon of rather uniform thickness, aside from a train of quite regularly spaced surface waves in the process of rolling up. As the beam density is further reduced (Figs. 15c, 15d), the cocoon thickness increases to 5-10 times the beam radius, while surface waves assume a more complex character. The same qualitative behavior is seen to hold for the sequence of Mach 12 jets in Figures 11d-14d. Thus, as jet density decreases we have a trend from naked beams to thick cocoons.

This morphological trend is a consequence of the strong dependence of backflow on beam density. Backflowing gas is shown in white in Figure 15, and can be seen to be absent in dense jets but to dominate the cocoons of diffuse jets. Simple arguments can be made to show why a dense jet should have forward-moving waste matter and a diffuse jet backward-moving waste matter. Note however that forward-flowing gas is also found in the cocoons of diffuse jets (Figs.15c,d). This derives from large-scale eddies in the cocoon that are associated with surface waves (NSWS, Fig.7).

At lower Mach numbers the same basic cocoon thickness trend is present (cf. Figs.3d,4d and Figs.5d,6d), although more striking morphological differences emerge that are related to interfacial instabilities at the working surface and on the cocoon and beam boundaries. Figure 3 shows pinch instabilities of a naked beam with a small amount of

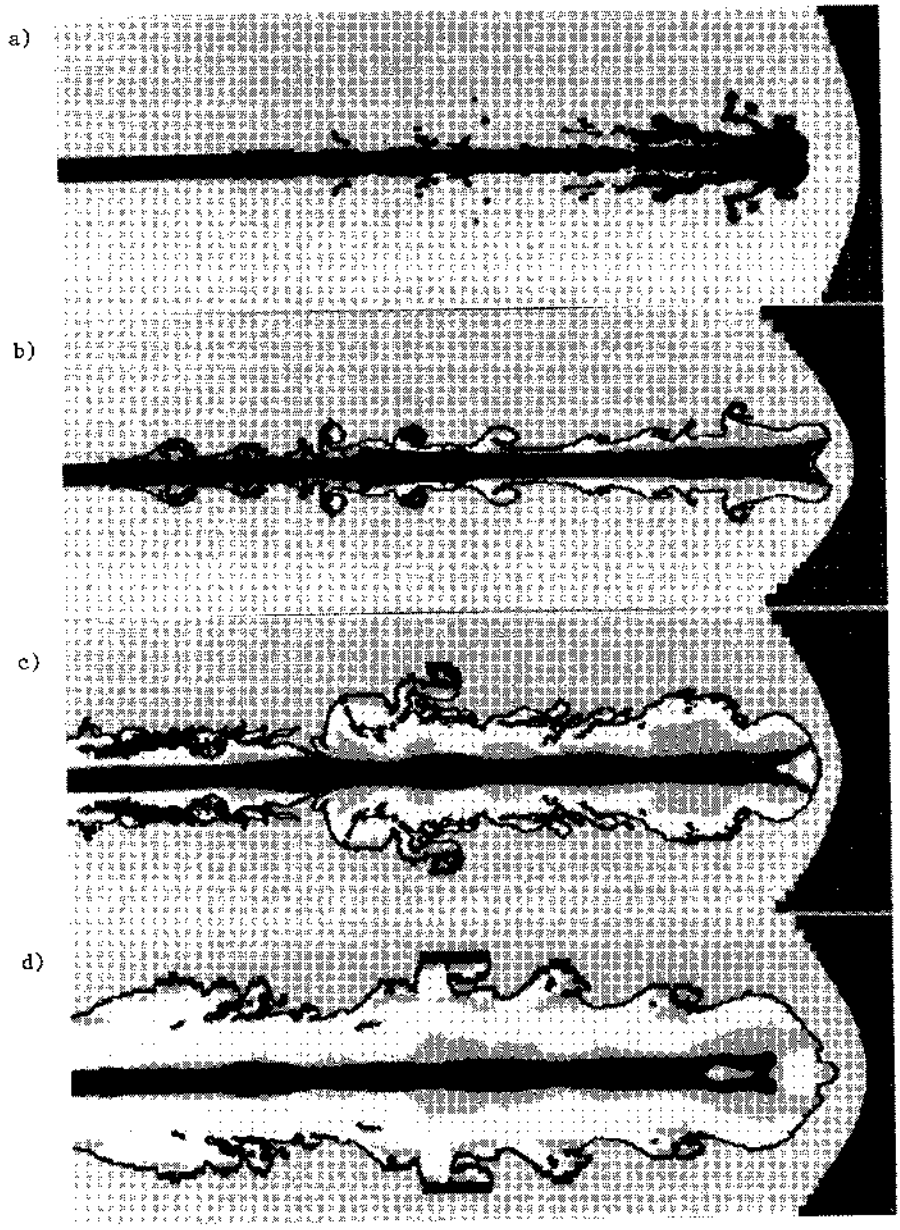


Figure 15. Naked beams and thick cocoons: a sequence of Mach 6 jets having different densities. a)ρ_b/ρ_m = 10, b) ρ_b/ρ_m = 1, c) ρ_b/ρ_m = 0.1, d) ρ_b/ρ_m = 0.01. Backflow (white regions) is stronglydependent on density.

accumulated material at the head. Figure 4 shows at early times a stable beam feeding a growing forward lobe which deflates at later times when the beam is pinched off. In Figure 5, a lobe is established, is turned over, and is sheared into sheets. Figure 6 shows cocoon turnover and mixing via the Kelvin-Helmholtz instability, which leaves only a forward lobe intact. As one goes back along the jet towards the source, cocoon gas and confining gas have been more thoroughly mixed because they have had more time to turn over than nearer to the head. This is in sharp contrast to the behavior in a subsonic plume, where gas at the head has mixed the most.

Figure 16 displays how gross morphology changes with Mach number for a sequence of jets having the same beam density. The tendency at low Mach numbers is for the waste matter to be concentrated in a lobe near the working surface, while at higher Mach numbers the waste matter is more evenly distributed along the length of the jet. Figures 16c and 16d show that extensive cocoons are the result of backflow. We argue in NSWS, section VI that backflow strength scales as M_b^2, and determines how far waste matter can be transported away from the head of the jet. An additional factor when one compares jets of the same length, is that at high Mach numbers the surface instabilities have had less time to grow and gobble up the cocoon than at low Mach numbers. The important modes of instability may also be different.

Having now examined jet morphology and how it depends on position in the theoretical plane, we can attempt to relate this to propagation efficiency. The relationship is easily found: the most slender jets propagate with the highest efficiency, and the thickest, most blunt-nosed jets propagate with the lowest efficiency. The minimum in η near Mach 3 is related to the propensity of these jets to develop blunt, or even concave nose geometries which persist in time (cf. Figs.5 and 6). Sometimes it is unclear which is cause and which is effect. Does a low propagation efficiency imply a blunt nose, or vice-versa? Consider the evolution of the jet in Figure 8, which displays a "breathing" mode which is seen to be quite regular on the basis of the surface waves it leaves behind.

Two final trends in the data deserve note. The first is jet "bloating" - the secular increase in jet thickness as it advances. This is best illustrated in Figure 10, and seems to be a property of the most powerful jets (cf. Figs.9, 10,13,14). Bloating would occur if the head of the jet were to decelerate, while all the while receiving the same throughput from the beam. There is a strong correlation between bloating and the deceleration parameters in Table 1. The most powerful jets have the strongest backflow (diffuse, high Mach number jets), and bloating would also occur when the backflow is choked by penetrating cocoon instabilities, as appears to be happening in Figures 9d and 13d.

The second trend concerns where the beam energy is deposited. In Figur 15 we see that the beam terminates further and further from the leading contact surface as beam density decreases. In Figure 16 we see

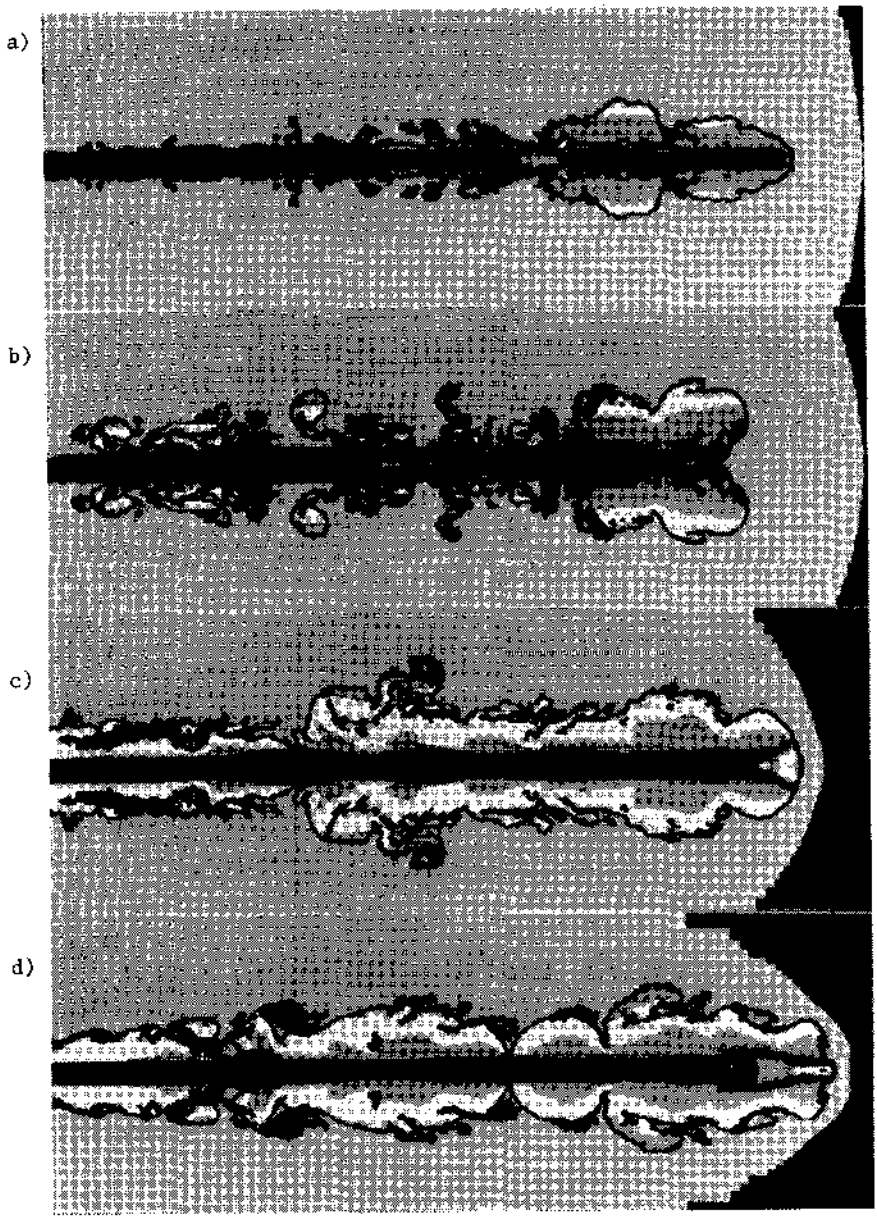


Figure 16. Lobes and unstable cocoons: a sequence of $\rho_b/\rho_m = 0.1$ jets having different Mach numbers. a) $M_b = 1.5$, b) $M_b = 3$, c) $M_b = 6$, d) $M_b = 12$ Backflow (white regions) is strongly dependent on Mach number.

the same trend as beam Mach number increases. Thus we find that high-powered beams dump their energy further from the jet end than low-powered beams.

6. SUMMARY

To summarize, we have studied the propagation and gross morphology of a 2-parameter family of pressure-confined supersonic jets. Propagation efficiency η, defined with respect to the usual ram-pressure estimate, is high for jets advancing sonically into the undisturbed medium. As the beam Mach number M_b increases away from unity, and holding the beam density ρ_b constant, η first decreases reaching a minimum around $M_b = 3$, and then increases. Holding M_b constant, η increases with ρ_b. We also find systemeatic trends in the gross appearance of jets of varying density and Mach number. Dense jets ($\rho_b > \rho_m$) are kinematically the simplest and consist of only a beam in direct contact with the confining medium. Holding Mach number fixed, as beam density is reduced, the trend is from naked beams to jets with thick, backflow-dominated cocoons. Holding beam density fixed, as Mach number is reduced, the trend is from extensive cocoons to lobes of waste matter localized near the head of the jet. Thin, dense jets propagate most efficiently ($\eta \gtrsim 0.8$), while thick, diffuse jets propagate the least efficiently ($\eta \lesssim 0.4$).

ACKNOWLEDGEMENTS

One of us (L.S.) wishes to acknowledge partial financial support from the National Science Foundation under grant no. PHY 80-01496.

REFERENCES

Blandford, R.D., Begelman, M.C., and Rees, M.J. 1982, Scientific American 5, 84.

Blandford, R.D., and Rees, M.J. 1974, Monthly Notices Roy. Astron. Soc. 169, 395.

Harlow, F.H., and Fromm, J.E. 1965, Scientific American 3, 104.

Hjellming, R.M., and Johnston, K.J. 1981, Ap. J. (Letters) 246, L141.

Love, E.S., Grigsby, C.E., Lee, L.P., Woodling, M.J., 1959, NASA Technical Report TR-R-6.

Norman, M.L., Smarr, L., Winkler, K.-H.A., and Smith, M.D. 1982, Astron. Astrophys. 113, 285.

Norman, M.L., and Winkler, K.-H.A. 1983, to appear in Astrophysical Radiation Hydrodynamics, ed. K.-H.A. Winkler and M.L. Norman, D. Reidel.

Woodward, P., and Colella, P. 1983, accepted J. Comp. Phys.

DISCUSSION

M. BEGELMAN: Do any of your lower Mach number jets break up after travelling a certain distance.

M. NORMAN: Yes. Our Mach number = 1.5 jets break up; however, under the assumption of axisymmetry, jet "break-up" proceeds in perhaps an unrealistic fashion. Unstable Kelvin-Helmholtz modes on the surface of the beam grow to the point of chopping off the beam in the form of thin fingers of external gas. The fingers are subsequently shattered by the Rayleigh-Taylor instability as they are accelerated by the beam thrust. External gas is thus entrained into the beam in this form of disruption. Now, since the growth rates of the helical modes are similar to the pinching modes for these parameters, we would expect disruption in the general case to be non-axisymmetric, but nontheless involving significant entrainment of external gas.

M. NEPVEU: Did you perform calculations using half the usual resolution? Motivation: does a Kelvin-Helmholtz instability such as found by you scale down? Is λ independent of the grid used?

M. NORMAN: When computing with half resolution, Kelvin-Helmholtz modes that are still adequately resolved (i.e. $\sim$ 20 zones/wevelength) are quite unaffected. However modes that are marginally resolved at higher resolution are numerically damped. This is the case that the λ of the dominant mode is either independent of the grid, or the mode disappears altogether and the flow is stable.

G. BENFORD: In M87 we know that the X-ray synchrotron implies a substantial magnetic field. How would that affect (qualitatively!) your periodic shock-produced knots?

M. NORMAN: In a fundamental sense, long trains of well-spaced shocks should arise whenever the beam is causally out of contact with its immediate environment. In pure fluid beams this means supersonic flows. So I would expect the same qualitative behaviour in supermagnetosonic flows in $B_{\perp}$ beams, or superAlfvenic flows in $B_{\parallel}$ beams.